JOURNAL OF Applied Polymer SCIENCE

Novel Preparation Method for Enhancing Nanoparticle Dispersion and Barrier Properties of Poly(ethylene terephthalate) and Poly(*m*-xylylene adipamide)

Yin Wang, Saleh A. Jabarin
Polymer Institute and Department of Chemical and Environmental Engineering, University of Toledo, Toledo, Ohio 43606-3390
Correspondence to: S. A. Jabarin (E-mail: saleh.jabarin@utoledo.edu)

ABSTRACT: A modified melt blending method has been developed for preparing exfoliated nanocomposites of poly(ethylene terephthalate) with sodium-montmorillonite (Na-MMT) and poly(*m*-xylylene adipamide) with Na-MMT. In this novel compounding process, a Na-MMT water solution was blended with the polymer in a twin screw extruder. This mixing process ensured that the silica nanoparticles were exfoliated in the polymer matrix through fixing the nanoparticles within the polymer matrix almost as they were in water. Transmission electron microscopy (TEM) and X-ray diffraction were used to determine nanoparticle dispersion level. The absence of the X-ray basal reflections in conjunction with the TEM images revealed the exfoliation of clay platelets. Differential scanning calorimetry illustrated that the nucleating abilities of montmorillonite were related to clay content and dispersion morphology. Oxygen permeation results indicated that the improved morphologies had enhanced the barrier properties of the nanocomposites.
 J. Appl. Polym. Sci. 129: 1455–1465, 2013

KEYWORDS: clay; polyesters; X-ray; composites; microscopy

Received 2 May 2012; accepted 18 November 2012; published online 12 December 2012
DOI: 10.1002/app.38853

INTRODUCTION

Polymer-clay nanocomposites have attracted strong interest within the packaging industry, because they may provide potential advantages over conventional polymers.[1,2] The use of nanoparticle instead of microparticle dispersions is expected to result in property improvements, since the majority of physical and chemical interactions would be dominated by clay-polymer surface properties.[3–5] The addition of nanoparticles to polymers used for food and beverage containers may lead to improved barrier properties, which would extend the shelf life of products and improve material stiffness and dimensional stability. Many researchers have focused on preparing nanocomposites with organically modified and unmodified clay.[6–15] Generally, three main preparative strategies; including *in situ* polymerization,[16–20] melt blending,[21–24] and solution intercalation[25,26]; have been used for incorporation of nanoclays into polymer matrices. Nanocomposites may be tactoid, intercalated or exfoliated, based on the clay dispersion state in the polymer matrix. The key objective for production of improved polymer-clay nanocomposites is to obtain high levels of exfoliation, because well dispersed structures are expected to provide the most improved properties in nanocomposite materials.[27–30] Two important factors, including surface organo-modification[31–33] and extrusion conditions[34–36] (shear rate, temperature, screw speed, residence time, and screw configuration) have been investigated in relationship to clay exfoliation. The majority of reported results concerning PET nanocomposites indicate that in most cases mixed intercalated and exfoliated morphologies have been achieved.[37–40]

Poly(ethylene terephthalate) (PET) is a semicrystalline thermoplastic polymeric material with a good balance of thermal, mechanical, and barrier properties.[41,42] Poly(*m*-xylylene adipamide) (MXD6) is another semicrystalline thermoplastic that shows high oxygen barrier properties, good transparency, high mechanical strength, and satisfactory heat resistance.[43,44] To further enhance the barrier properties, thermal stability and mechanical properties of PET and MXD6, nanoclays can be added into the matrices of these polymers. Several reports describe the processing and properties of PET and MXD6 nanocomposites prepared by either melt mixing or *in situ* polymerization methods.[16,17,21–24,30,45–49] Some of these studies have concentrated on dispersing organically modified clays in PET or MXD6, with results indicating various degree of exfoliation.[21,30,39] The organic modifiers, however, could not endure the high processing temperature required for engineering plastics and such exposure caused them to undergo thermal degradation.[10,24,33,39,50,51]

Previous evaluations of nanocomposites indicate that the dispersed clay acted as a nucleating agent for PET, and increased its crystallization rate.[23,52,53] Kim et al.[30] and Scaffaro et al.[39] studied the influence of different kinds of organically modified montmorillonite (OMMT) on the various properties of PET-based nanocomposites prepared by melt blending. Morphological studies showed that Cloisite 30B nanoparticles were more compatible with PET, because of their greater affinity with it, and achieved better dispersion in the polymer matrix, compared with Cloisite 10A and Cloisite 15A. At 3 wt % OMMT, oxygen permeation of the exfoliated PET/30B nanocomposite was reduced by 29% compared with that of PET. Kim and Huh[54] and Ghasemi et al.[21] investigated the effects of different thermally stable surfactants such as phosphonium, imidazolium, and pyridinium on the thermal stability of PET. They found that surfactant based nanocomposites exhibited better thermal stability than that of nanocomposites without surfactant, in addition to improving the dispersion level and mechanical properties of nanocomposites.

To avoid thermal degradation issues, more recent work followed an approach based on *in situ* polymerization, to prepare PET nanocomposites without organic modification.[55] Sodium-montmorillonite (Na-MMT) was dispersed in ethylene glycol and bis(2-hydroxyethyl) terephthalate (BHET) monomer by using appropriate solvents, before polymerization was carried out. The morphological results revealed that exfoliated and intercalated morphologies were obtained for PET/Na-MMT, and that PET nanocomposites produced by the esterification (ES) clay addition method showed more improvement in properties than nanocomposites prepared using the polycondensation clay addition method. The 0.5 wt % ES clay addition nanocomposite showed 36% oxygen barrier property improvement in comparison to neat PET.

As a continuation of the search for methods capable of achieving better exfoliation of nanoparticles in PET or MXD6 matrices, we present a new investigation of this topic. Specifically, this work includes development of a novel process for the preparation of PET/Na-MMT and MXD6/Na-MMT nanocomposite in which the Na-MMT is exfoliated at the nanometer level. The Na-MMT used for development of this process is without organo-modification. Because of its hydrophilic nature, it can be exfoliated in water to form clay dispersions. Past preparations of nanocomposites through dispersions of clay in water, were limited to hydrophilic polymers such as poly(vinyl alcohol).[56] In addition to the process development, this article reports dispersion results that have been examined using X-ray diffraction (XRD) and transmission electron microscopy (TEM) methods. Thermal and oxygen barrier properties have also been evaluated and are reported.

EXPERIMENTAL

Materials

Na-MMT was supplied by Southern Clay Products with a cation exchange capacity of 92.6 meq/100 g clay. Commercially available PET resin (grade HP806) with an intrinsic viscosity (IV) of 0.84 dL/g was obtained from Wellman Company and was used as the PET polymer matrix. MXD6 (Grade 6011) with a density of 1.2 g/cm^3 was obtained from the Mitsubishi Gas Chemical Company and was used as the MXD6 polymer matrix. All the materials were used without additional treatment, except for drying.

In preliminary efforts to obtain Na-MMT dispersions, 20 g of Na-MMT was added to 980 g of stirred room temperature deionized water (2 wt %). Time required for the stirring process was evaluated to ensure the clay particles were completely dispersed in the water. It was observed that the slurry was off-white in color and contained undispersed lumps of clay after stirring for time intervals ranging from 2 to 6 h. After 6 h of continuous stirring, a uniform dispersion of the clay in water was achieved. It was thought that faster clay dispersion could be achieved with the assistance of heat. Higher temperatures, such as 40 and 60°C were used in an attempt to shorten the preparation time for the clay dispersion; however, the higher temperatures were found to have no significant effects on the preparation time.

It is well known, that water present during the melt blending process could cause hydrolytic degradation of PET at high processing temperatures. To reduce the amount of water that was introduced into the extruder, another slurry composition with higher weight percent concentration of clay was prepared at room temperature. For this purpose, 40 g of Na-MMT was added to 960 g of deionized water (4 wt %) with continuous stirring. It was found that complete dispersion of clay in this slurry was obtained after 8 h of stirring. An additional attempt was made to further decrease the water content in the slurry; however, increasing the clay content to 5 wt %, made it difficult to disperse the clay due to formation of lumps. Results of the preliminary experiments, therefore, indicated that the clay water dispersion should be prepared with 4 wt % clay loading at room temperature. All subsequent Na-MMT slurries were dispersed in a water solution and stirred 15 h with a magnetic stirrer before the melt blending process.

The pump for dispersion of the clay slurry into the extruder was calibrated as follows. The motor of the pump was operated at different speeds. At each motor speed, the clay slurry was collected for 1 min and weighted. The actual feed rate of the clay slurry was plotted against the motor speed and it was found to be linear. The regulator monitoring resin feed rate to the extruder was calibrated in similar manner.

Prior to the extrusion process, the PET and MXD6 resins were each dried in a Conair dehumidifying air dryer at 140°C for 12 h. To prepare PET/Na-MMT and MXD6/Na-MMT nanocomposites by the melt blending process, the polymer resin and the Na-MMT slurry were simultaneously fed into the corotating twin screw extruder (ZSF-30). The feed rate of the PET or MXD6 resin was 100 g/m. Rates for the clay slurries were 12.5, 25, 50, 75, and 125 g/m to respectively give final nominal clay concentrations of 0.5, 1 (1.0), 2 (2.0), 3 (2.9), and 5 (4.8)% (wt/wt) after water removal. The screw speed was maintained at 200 rpm, and temperatures of zones one through five, as well as the exit die, were 280°C. Virgin PET or MXD6 pellets and the clay slurry were fed into the hopper of the extruder. As the clay slurry was mixed with molten polymer, much of the water was

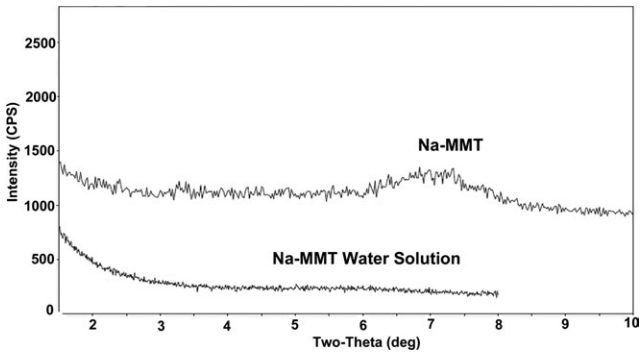

Figure 1. XRD patterns of Na-MMT powders and clay dispersion in water.

immediately volatilized from the nanocomposite through the extruder hopper and additional water was removed from the screw area of the extruder with a vacuum pump. Extruded strands exiting the die were immediately cooled in room temperature water, pelletized, and dried.

Solid state polymerization (SSP) was used to increase the molecular weights (as measured by melt viscosity) of the PET and MXD6 nanocomposites to equivalent levels. All the nanocomposite pellets were crystallized at 140°C for 2 h to avoid sticking during SSP. The crystallized nanocomposites were loaded into the SSP reactor (Buhler Company, Bühler AG, capacity 1 kg) and heated up to 220°C under a nitrogen environment for 5–8 h. (2000 L/h. flow rate, 0.3 bar pressure). During the SSP process, samples were collected at different time intervals to monitor changes in their melt viscosity.

The thin films of the nanocomposite were obtained for oxygen permeation evaluations with a laboratory scale Brabender single screw extruder (screw diameter $D = 19$ mm, $L/D = 22/1$, and compression ratio = 3/1) equipped with a cylindrical die. Prior to the extrusion the pelletized, SSP, nanocomposites were dried at 140°C in a vacuum oven for 12 h. Pellets were processed at an extrusion temperature of 280°C and 60 rpm. The molten polymer exited a die filled with nitrogen to obtain thin "balloon-like" films.

Characterization

Wide Angle XRD. XRD patterns were obtained with a Rigaku Ultima X-ray diffractometer (The Woodlands, TX) using Ni-filtered Cu Kα radiation (0.1541 nm wavelength) generated at 44 kV and 44 mA. Power and clay slurry samples were scanned in the interval of $2\theta = 2–8°$ at 0.5°/min. The interlayer spacing of the Na-MMT was derived from the Bragg equation.

Transmission Electron Microscopy. The morphologies of the nanocomposites were studied using TEM (Pleasanton, CA). The pelletized samples were sectioned using 45° glass or diamond knives at room temperature to obtain specimens of 100 nm thickness. The sectioned specimens were collected on 200 mesh grids. Transmission electron micrographs were obtained with a Hitachi HD-2300 (Schaumburg, IL) using an accelerating voltage of 200 kV.

Thermogravimetric Analysis. A TA instrument Q500 thermogravimetric analyzer (TGA; New Castle, DE) was used to measure the actual weight loading of clay in the PET and MXD6 matrix. The samples with weight between 5 and 10 mg were heated from room temperature to 1000°C at a rate of 5°C/min. Measurements were performed in triplicate for each sample, under 80 mL/min gas flow of air or nitrogen.

Melt Viscosity. Melt viscosities of the nanocomposites were measured with a Rheometric Scientific (RDA III) dynamic analyzer (Piscataway, NJ). Samples were loaded into the rheometer fixture with 1 mm parallel disks and evaluated at 280°C in the presence of a nitrogen purge. The melt viscosity values taken at 10 rad/s were converted to PET equivalent IV values according to the method described recently.[55]

Differential Scanning Calorimeter (DSC). Thermal properties of the SSP samples (8–11 mg) were evaluated with a Perkin-Elmer DSC 7 (Shelton, CT) under a dry nitrogen atmosphere. Samples were heated at a rate of 10°C/m from 40 to 300°C. They were then quenched to 40°C at a nominal rate of 300°C/m. The second heating was performed from 40 to 300°C at 10°C/min, followed by cooling to 40°C at 10°C/min. In addition, nonisothermal crystallization kinetics of PET, PET/Na-MMT (0.5 and 3 wt %), and MXD6/Na-MMT (3 wt %) were obtained from the molten states and observed at cooling rates of 5, 10, 20, 30, 40, 50, 60, 70, and 80°C/m.

Oxygen Permeability Measurements. Oxygen permeability evaluations of the SSP PET/Na-MMT and MXD6/Na-MMT nanocomposite films, with different clay contents, were performed using a MoCon OxTran 1050 permeability tester according to ASTM D3985. Samples were conditioned in nitrogen inside the unit for 24 h prior to being tested. The upper surface of PET and its nanocomposites were exposed to an air environment at 23°C and 45% RH while the lower surface was flushed by the carrier gas (98% N_2 with 2% H_2) at 23°C and 0% RH. In the case of MXD6 and its nanocomposites, samples were tested in a pure oxygen atmosphere rather than air to reduce testing time at 23°C and 0% RH.

RESULTS AND DISCUSSION

XRD patterns for Na-MMT, both as a dry powder and as water dispersion, are presented in Figure 1. As can be seen, the Na-MMT powder exhibits a characteristic diffraction peak with a d-spacing of 1.12 nm at $2\theta = 7.4°$. When Na-MMT is dispersed in distilled water, the absence of scattering angle peaks suggests that the natural clay platelets are exfoliated due to their

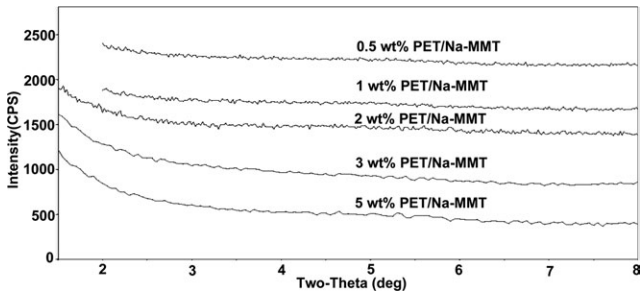

Figure 2. XRD patterns of PET/Na-MMT nanocomposites prepared at nominal concentration of 0.5, 1, 2, 3, and 5 wt % of clay in PET.

Applied Polymer SCIENCE

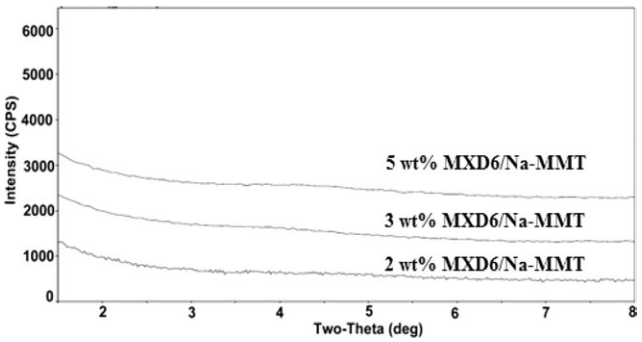

Figure 3. XRD patterns of MXD6/Na-MMT nanocomposites prepared at nominal concentration of 2, 3, and 5 wt % of clay in MXD6.

hydrophilic nature. Figures 2 and 3 give XRD patterns for the PET/Na-MMT nanocomposites (with nominal clay concentrations of 0.5, 1, 2, 3, and 5 wt %) and MXD6/Na-MMT nanocomposites (nominally containing 2, 3, and 5 wt % clay). The absence of basal reflections in the X-ray patterns for both types of nanocomposites indicates the formation of exfoliated nanostructures. Similar results were reported by Cho and Paul.[57] They described the preparation of nylon 6/Na-MMT by melt blending and investigations of its morphological properties. They concluded that the absence of clay diffraction peaks was strong evidence for the formation of an exfoliated nanocomposite. In the work of Zhao and Samulski,[58] XRD was used to indicate the d-spacing of poly(methyl methacrylate) and polystyrene/clay nanocomposites. Their results showed that the clay was nearly exfoliated in both polymers, based on disappearance of the characteristic peak.

To verify the results obtained from the current XRD data, TEM was used to image the morphological structures of the prepared samples. Figure 4(a–e) shows the TEM photomicrographs of PET nanocomposites respectively containing 0.5, 1, 2, 3, and 5

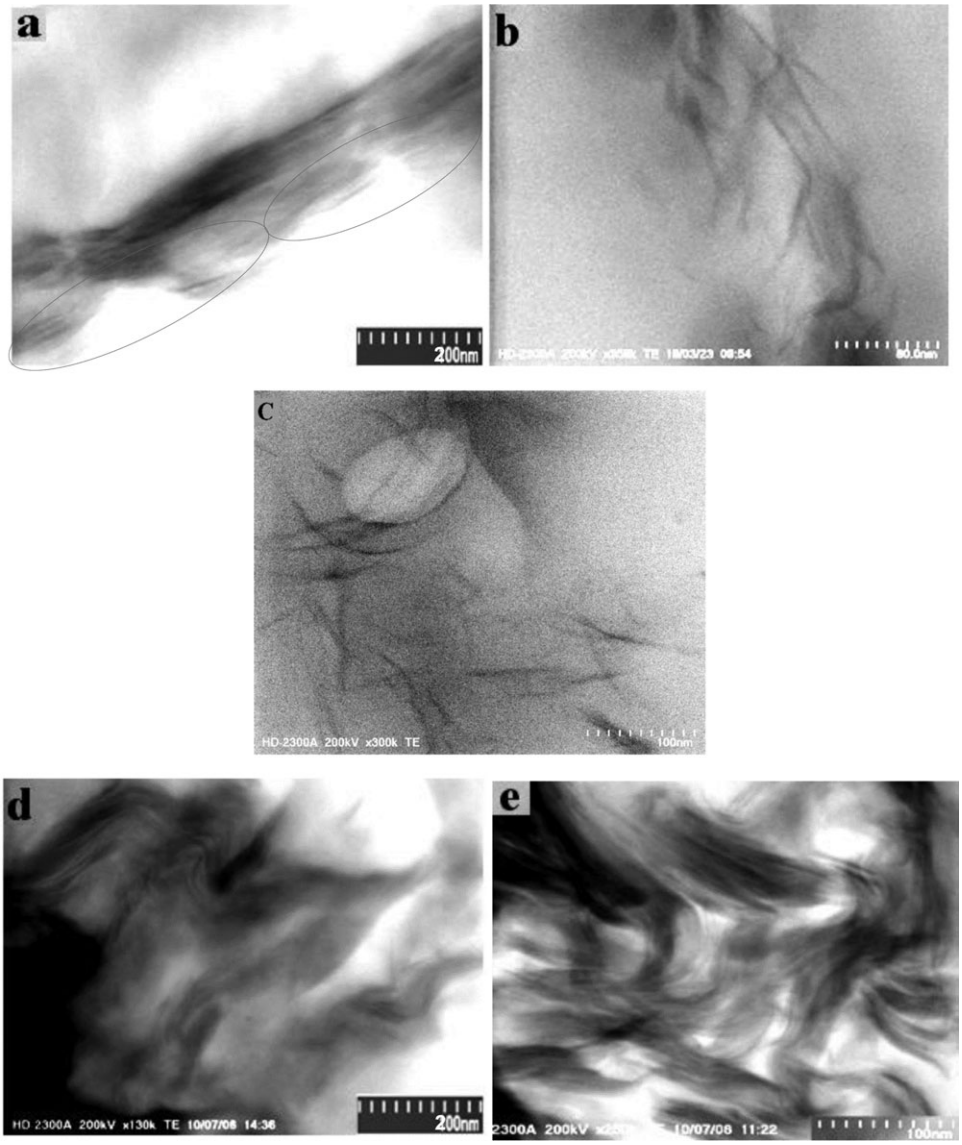

Figure 4. TEM images of PET/Na-MMT nanocomposites prepared with the NaMMT concentration of (a) 0.5 wt %, (b) 1 wt %, (c) 2 wt %, (d) 3 wt %, and (e) 5 wt %.

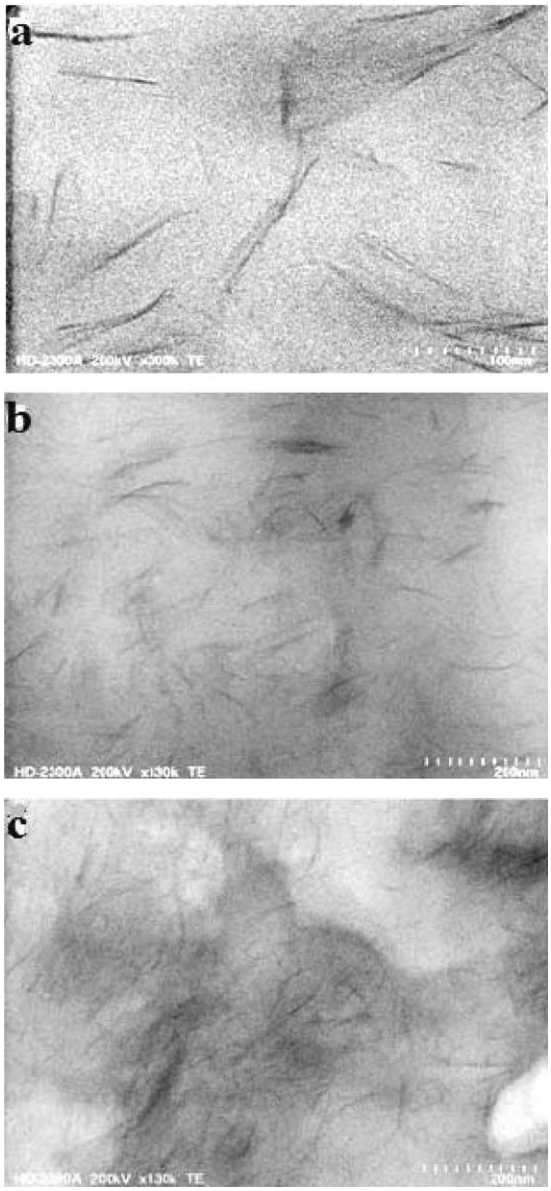

Figure 5. TEM images of MXD6/Na-MMT nanocomposites prepared with the NaMMT concentration of (a) 2 wt %, (b) 3 wt %, and (c) 5 wt %.

wt % Na-MMT. The black lines in the pictures correspond to the clay layers, while the lighter background represents the polymer matrices. The nanoparticles were very widely dispersed at the lowest 0.5% concentration making them difficult to locate with TEM. In Figure 4(a), ellipses indicate the most clearly visible exfoliated nanoparticles. The dark area above the ellipses is a thicker portion of the PET matrix. In Figure 4(b,c), the Na-MMT is clearly seen to be highly dispersed in the PET matrix indicating exfoliated morphology of the clay layers. The morphologies of Figure 4(d,e) show mixtures of high levels of intercalated and partially exfoliated features. Other studies have used a clay supported catalyst approach,[59] which resulted in intercalated nanocomposite structures. Figure 5(a–c) displays TEM images of MXD6/Na-MMT nanocomposites, respectively, containing 2, 3, and 5 wt % nominal clay concentrations. The micrographs of all of the MXD6 nanocomposites reveal well exfoliated structures.

The TEM results indicate that XRD observations should not be the only route used to confirm the morphology of nanocomposites. The disappearance of diffraction peaks may indicate intercalation or exfoliation of the clay.[60–62] Eckel et al.[61] evaluated organo-clay dispersions in polymer nanocomposites using XRD and TEM. They found that XRD was somewhat limited in quantifying clay dispersions, since mixed layering, and other peak broadening factors could cause the disappearance of the diffraction peak, as has also been discussed by Morgan and Gilman[62] Results of the current morphological studies indicate that at lower clay loading, Na-MMT has been effectively exfoliated in both PET and MXD6 nanocomposites. These results also indicate that XRD should be combined with TEM to confirm the actual clay dispersion within the polymer.

TGA can measure changes in the weight of a material as a function of temperature in a controlled atmosphere, to determine its composition. In this study, levels of the nonvolatile clay residues of the PET/Na-MMT and MXD6/Na-MMT nanocomposites were evaluated with TGA, to obtain the values shown in Table I. In addition to the TGA results, the table gives nominal clay concentrations of the nanocomposites as well as their calculated concentrations. Previous work by Patro et al.,[63] reported that when unmodified Cloisite Na+ was heated in a TGA, the mass loss below 200°C represented evaporation of free water and that mass loss between 500 and 800°C indicated loss of structural water. They reported that the total mass lost over the whole temperature range was 12.4%. Table I also contains a column showing calculated nanocomposite clay concentrations with all (12.4%) free and structural water removed. It can be seen that the inorganic residuals remaining after complete TGA combustion of the nanocomposites are similar to the calculated values

Table I. TGA Measurements of Clay Concentrations in Nanocomposites, % (wt/wt)

Nominal clay concentration (%)	Calculated clay concentration (%)	Calculated clay residue with all water removed (%)	TGA measured nonvolatile residue (%)	
Clay	Clay	Clay	Na-MMT/PET	Na-MMT/MXD6
0.5 wt %	0.50	0.43	0.42 ± 0.015	-
1 wt %	0.99	0.87	0.9 ± 0.020	-
2 wt %	1.96	1.72	1.6 ± 0.017	1.7 ± 0.021
3 wt %	2.91	2.55	2.3 ± 0.029	2.5 ± 0.015
5 wt %	4.76	4.17	3.9 ± 0.015	4.1 ± 0.025

Table II. Initial I.V and SSP I.V Values for Nanocomposites of PET and MXD6

	PET/Na-MMT I.V. (dL/g)		MXD6/Na-MMT I.V. (dL/g)	
Nominal clay loading	Initial	After SSP	Initial	After SSP
0.5 wt %	0.67	0.80	-	-
1 wt %	0.61	0.78	-	-
2 wt %	0.56	0.83	0.55	0.79
3 wt %	0.50	0.82	0.50	0.82
5 wt %	0.45	0.84	0.46	0.80

with all water removed. The small differences may be due to loss of clay during the process of the mixing it into the polymer in the twin screw extruder as reported by others.[64]

SSP was used to increase the molecular weight (as measured by melt viscosity) of the extruded nanocomposites to PET equivalent melt IV levels of about 0.8 dL/g. During the SSP process, samples were collected at different time intervals to monitor changes in their melt viscosity. Table II gives the initial equivalent melt I.V. values from the extruder and after SSP for PET/Na-MMT and MXD6/Na-MMT nanocomposites. Incorporation of low clay concentrations into the polymer was assumed to have negligible effect on the nanocomposite melt viscosity. Kim et al.[30] compared IV values for PET samples with and without clay to melt rheology results and found that data points for samples containing 3% clay fell on the same straight line as PET samples without clay. The melt viscosity measurements were done primarily to provide a tool for comparing the relative sample values to evaluate equivalent nanocomposite samples in terms of their thermal and oxygen barrier properties.

Crystallization behaviors of polymer nanocomposites have been the focus of extensive studies.[23,24,31,38,47,50–53,61,62] This is because the crystallization behavior influences the semi-crystalline structure of a polymer, which in turn affects the polymer's properties. Crystallization rate can be increased by the addition of nanoparticles that act as nucleating agents.[46,47,53,61,65,66] It is important to study the influence of Na-MMT on the crystallization and thermal behavior of PET and MXD6 to understand how to optimize processing conditions and properties of the polymer nanocomposites.

Thermal data in Table III and Figure 6 show the characteristic behaviors of PET and PET nanocomposites. All the samples have similar melt viscosity values, which reduces the influence of molecular weight differences on the crystallization behaviors of the PET nanocomposites. In the second heating scans, as shown in Figure 6(a), the quenched samples are heated from 40 to 300°C at 10°C/min. Table III shows the thermal properties of the composites. The glass transition temperatures (T_g) of the nanocomposites are slightly increased from 78 to 79.7°C. This may result from the addition of clay into the polymer matrices, which could inhibit the mobility of chain segments and also increase the crystallinity of samples. The melting temperatures (T_m) of PET nanocomposites shift to slightly higher temperatures and these slight increases may result from the hindrance to chain mobility caused by the nanoparticles in the PET matrix. Mucha et al.[67] reported that the T_m of polypropylene increased from 2 to 4°C as a result of the addition of carbon black particles. The heats of fusion (ΔH_m) of all the PET nanocomposites have been normalized for their nominal clay contents and are listed in Table III. The nanocomposite values are slightly higher ($\sim$ 2 J/g) than that of neat PET and these differences are more significant with increased clay concentrations. It can be seen that most of the nanocomposites (2, 3, and 5 wt %) crystallized during the quenching step, as these samples do not exhibit any significant crystallization peaks during reheating.

As shown in Table III, during reheating, the pure PET gives an enthalpy of crystallization (ΔH_c^m) of 22.5 J/g and an enthalpy of melting (ΔH_m) of 32.1 J/g. The difference between melting and crystallization enthalpies is 9.6 J/g, indicating the level of crystallization that occurred during the quenching process. For 0.5 and 1 wt % PET nanocomposite, about 80% of the total crystallinity is formed during the quenching process. With increased clay content, this disappearance of the crystallization peak during reheating results from the strong nucleating function of the clay, which increases the crystallization rate during the quenching process.[23,55]

All the PET nanocomposites shown in Figure 6(b) were cooled from 300 to 40°C at 10°C/min. The crystallization peak temperatures (T_c^c) of the PET nanocomposites occur at higher

Table III. Normalized DSC Results of PET and PET/Na-MMT Nanocomposites

	Reheating					Cooling			
Sample	Intrinsic viscosity (dL/g)	T_g (°C)	ΔH_c^m (J/g)	T_m (°C)	Modified ΔH_m (J/g)	T_{on}^c (°C)	T_c^c (°C)	$t_{1/2}$ (min)	ΔH_c^c (J/g)
PET	0.84	78.0	22.5	245.9	32.1	196.2	187.2	0.90	32.1
PETN 0.5 wt %	0.80	78.4	8.2	245.2	33.5	199.9	193.5	0.64	33.6
PETN 1 wt %	0.78	78.8	2.3	246.5	33.1	200.9	194.8	0.61	32.5
PETN 2 wt %	0.83	79.6	-	246.9	33.6	198.4	192.2	0.62	31.5
PETN 3 wt %	0.82	79.7	-	247.1	34.1	199.4	192.8	0.66	31.4
PETN 5 wt %	0.84	79.7	-	247.6	34.5	201.5	195.5	0.60	29.8

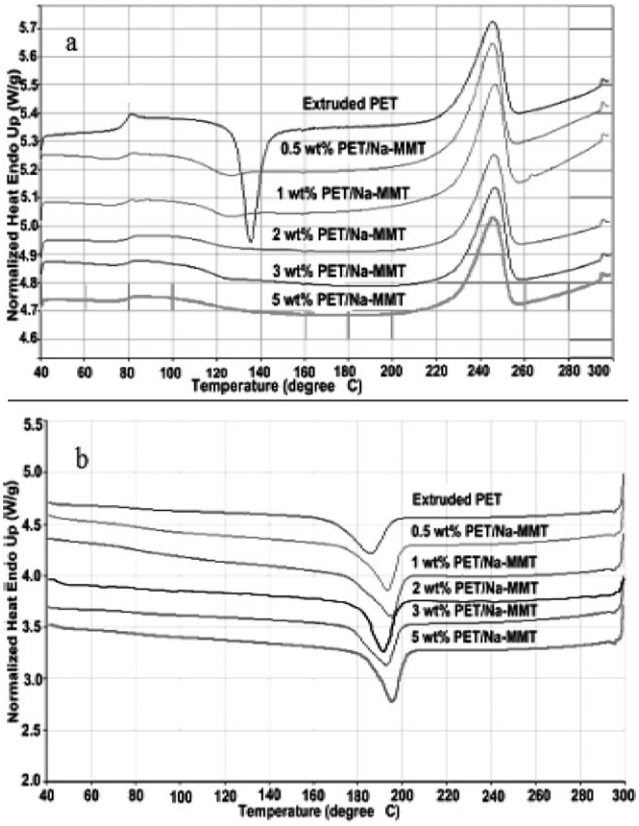

Figure 6. DSC curves of PET and PET/Na-MMT nanocomposites obtained at a constant rate of 10°C/min during: (a) reheating and (b) cooling.

temperatures compare with that of PET. The maximum T_c^c is 195.5°C for the 5 wt % clay content. The onset of crystallization temperature (T_{on}^c) also shifts to higher temperatures indicating that PET starts to crystallize sooner with increased clay addition, because of its strong nucleation effect.[47,55,64–66,68–70] Since the crystallization peaks obtained during cooling are symmetrical, their half times ($t_{1/2}$) of crystallization can be obtained using the following equation.[55,71]

$$t_{1/2} = (T_{on}^c - T_c^c)/\chi \quad (1)$$

Here T_{on}^c is the onset crystallization temperature (°C), T_c^c is the crystallization temperature at the exothermic peak (°C), and χ is the cooling rate (°C/min).

The half time of crystallization is an indicator of the overall crystallization rate attributed to the combined effects of nucleation and crystal growth. Table III includes crystallization $t_{1/2}$ values for PET and its nanocomposites. The crystallization half time ($t_{1/2}$) of PET is 0.9 min. Samples in which MMT has been incorporated exhibit a much lower average value of 0.62 min. These results indicate that the presence of clay acts as a heterogeneous nucleating agent stimulating the crystallization to occur sooner.[72–74] There are no significant differences in $t_{1/2}$ among nanocomposites with different clay contents. It appears that when well dispersed structures in PET nanocomposites are formed, this leads to similar crystallization behaviors and thermal characteristics.

Thermal properties obtained for the MXD6 and MXD6/Na-MMT nanocomposites are summarized in Table IV and shown in Figure 7. In the second heating scans, as seen in Figure 7(a), the T_g increases slightly in the nanocomposite samples in comparison to the value recorded for neat MXD6. This can be attributed to a higher rigidity in the amorphous phase of the polymer in the presence of the clay particles that restrict the molecular motions of the MXD6 chain segments.

Similar to the PET nanocomposites, normalized heats of fusion (ΔH_m) and T_m for MXD6 and its nanocomposites did not vary significantly with clay loading from 2 to 5 wt %. In contrast to PET nanocomposites, all MXD6 nanocomposites gave a crystallization peak during the reheating process. This occurred because most of the MXD6 matrix remained in the amorphous state during cooling. In the presence of Na-MMT, the crystallization enthalpies are reduced to about 20 J/g compared with 36 J/g for neat MXD6.

In the cooling process, as presented in Figure 7(b) and Table IV, Na-MMT added to MXD6 causes the crystallization peak temperature T_c^c for all three concentrations to occur at higher temperatures with shorter $t_{1/2}$ in comparison to the neat MXD6. At 10°C/min cooling rate, the $t_{1/2}$ values for the MXD6 nanocomposites are between 0.84 and 0.89 min. These are lower than that of MXD6, signifying that the addition of Na-MMT can accelerate the overall crystallization process.[75–79] The same conclusion could be observed from Figure 7(b); the crystallization peak of neat MXD6 in the cooling scan is broader, while the nanocomposites show narrower and sharper peaks. For the MXD6 nanocomposites (2, 3, and 5 wt %), both onset of crystallization temperatures and half times of crystallization are independent of clay content, implying similar nanostructures. These observations further verify the TEM results, that all the

Table IV. Normalized DSC Results of MXD6 and MXD6/Na-MMT Nanocomposites

	Reheating				Cooling			
Sample	T_g (°C)	ΔH_c^m (J/g)	T_m (°C)	Modified ΔH_m (J/g)	T_{on}^c (°C)	T_c^c (°C)	$t_{1/2}$ (min)	ΔH_c^c (J/g)
MXD6	84.7	36.4	238.2	64.6	187.3	173.5	1.38	46.1
MXD6N 2 wt %	85.4	19.4	238.2	59.1	192.3	183.9	0.84	46.3
MXD6N 3 wt %	85.9	20.8	238.3	57.8	191.4	182.5	0.89	44.8
MXD6N 5 wt %	85.1	29.3	237.9	64.8	192.2	183.5	0.87	46.2

Applied Polymer SCIENCE

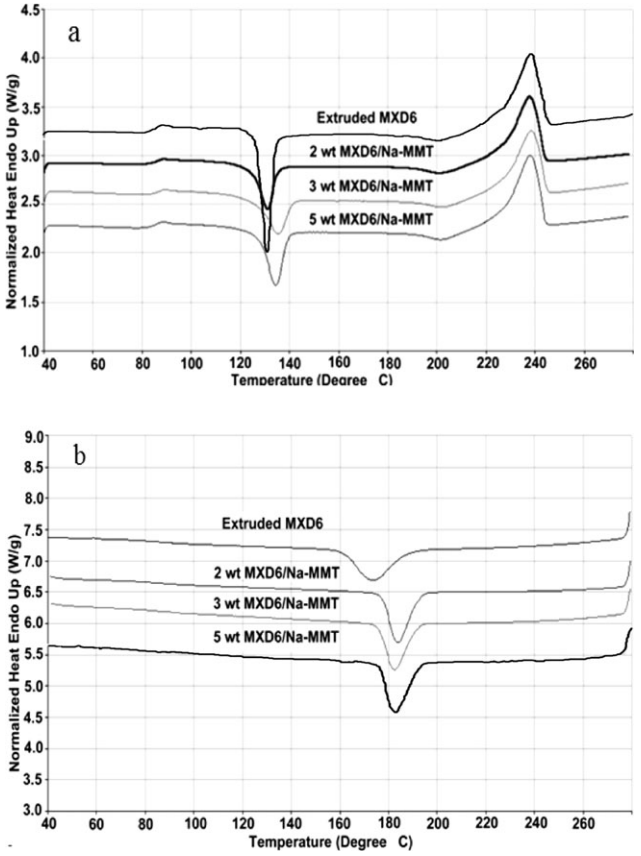

Figure 7. DSC curves of MXD6 and MXD6/Na-MMT nanocomposites at a constant rate of 10°C/min (a) reheating and (b) cooling.

MXD6 nanocomposites prepared in this work achieved primarily exfoliated morphologies.

In the reheating process, the absence of crystallization peaks for PET nanocomposites show that different crystallization behavior is occurring for PET nanocomposites, during the quenching process. To more fully investigate the differences of crystallization behavior among these nanocomposites, sample of PET, as well as 0.5 and 3 wt % PET/Na-MMT nanocomposites were examined at eight different cooling rates. The work was done to

Table V. Normalized DSC Data for PET Nanocomposites Cooled at Different Rates

		ΔH_c^c (J/g)		
Cooling Rate (°C/min)	1/CR (min/°C)	PET	PET/NaMMT 0.5 wt %	PET/NaMMT 3 wt %
5	0.2000	35.2	35.5	32.9
10	0.1000	31.9	32.4	30.6
20	0.0500	24.2	31.5	29.8
40	0.0250	9.1	30.7	27.5
50	0.0200	3.7	23.7	26.4
60	0.0170	3.6	16.5	22.7
70	0.0140	2.8	13.8	20.4
80	0.0125	2.6	8.8	19.2

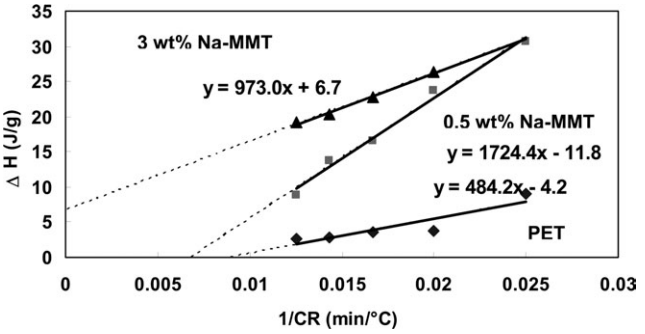

Figure 8. Extrapolated curves of PET and PET/Na-MMT nanocomposites obtained at cooling rates of 40, 50, 60, 70, and 80°C/min.

investigate further the crystallization behavior observed among PET nanocomposites during the faster quenching process.

A summary of the non-isothermal crystallization behaviors of extruded PET, 0.5 and 3 wt % PET/Na-MMT nanocomposites is given in Table V. As expected, the crystallization enthalpies (ΔH_c^c), normalized in terms of nominal clay contents, decrease with increased cooling rate for PET and its nanocomposites. Higher cooling rates give less time for polymer chains to fold and crystallize. The shorter times to complete the crystallization process result in the lower crystallization enthalpies. Figure 8 shows crystallization enthalpies ΔH_c^c plotted as functions of the reciprocals of their cooling rates. After extrapolation of the line to the X axis, as seen in Table VI, for extruded PET, the material is projected to remain completely amorphous at faster cooling speed. Similarly, it is shown that 0.5 wt % PET nanocomposite can be quenched into the amorphous state at a cooling rate of 147°C/min, slightly higher than that of extruded PET. In the case of the 3 wt % PET/Na-MMT nanocomposite, the material crystallizes even when quenched at an infinite rate. That is the reason for the diminishment of the crystallization peak observed during reheating as shown in Figure 6(a).

As indicated in Figures 6 and 7, the 3 wt % MXD6/Na-MMT nanocomposite shows a crystallization exotherm upon heating from a quenched state while its 3 wt % PET/Na-MMT nanocomposite equivalent does not show an exothermic peak. To further investigate the difference between these two nanocomposites, the MXD6 nanocomposite samples were cooled from melt at different cooling rates (Table VII). Figure 9 gives the dependence of its ΔH_c^c values plotted as functions of reciprocals of the cooling rates. The data show that, an amorphous state can be reached at a cooling rate of about 130°C/min. That is

Table VI. Crystallization Behavior of PET and Its Nanocomposite at Different Cooling Rates

Condition	Sample	Intercept
Amorphous	PET	0.0087 (115°C/min)
Amorphous	PET/Na-MMT 0.5 wt %	0.0068 (147°C/min)
Partially Crystallized	PET/Na-MMT 3 wt %	–

Table VII. Normalized DSC Data for 3 wt % MXD6 Nanocomposites Cooled at Different Rates

Cooling Rate (°C/min)	1/CR (min/°C)	ΔH_c^c (J/g)
5	0.2000	43.7
10	0.1000	43.0
20	0.0500	40.8
40	0.0250	35.3
50	0.0200	24.5
60	0.0170	12.4
70	0.0140	7.6
80	0.0125	4.5

the reason for the presence of the crystallization peak in reheating scans for 3 wt % MXD6 nanocomposite. This behavior is consistent with observed results for reheating scans of both MXD6 and PET nanocomposites.

Polymer nanocomposites are multiphase systems in which different diffusion and sorption can result in complicated transport phenomena.[80] The presence of impermeable inorganic fillers in a polymer matrix cause decreases in permeability of oxygen, because the fillers create more tortuous paths through the polymer.[81–84] Permeation evaluations have revealed that gas barrier properties were significantly improved for polymers containing exfoliated structures with high aspect ratios and better polymer surface interfacial adhesion.[84–86]

Table VIII gives oxygen permeability values recorded for amorphous films of PET and the PET/Na-MMT nanocomposites. It can be seen that the oxygen permeability of PET/Na-MMT nanocomposites decreased with increased clay loading. The largest reduction was observed at 2 wt % PET/Na-MMT, which gave a 52% improvement in its oxygen barrier compared to neat PET resin. The 5 wt % composition; however, only exhibited a reduction of 37%. This difference may have been related to the presence of tactoid structures as shown in the TEM image [Figure 4(e)]. In the work described by Frounchi and Dourbash,[87] two different organoclays (Cloisite and Nanolin) were prepared for PET nanocomposites using a melt blending method. The Nanolin nanocomposite showed a permeability, which was about half that of the pure PET, and the Cloisite nanocomposite showed a 30% barrier property improvement.

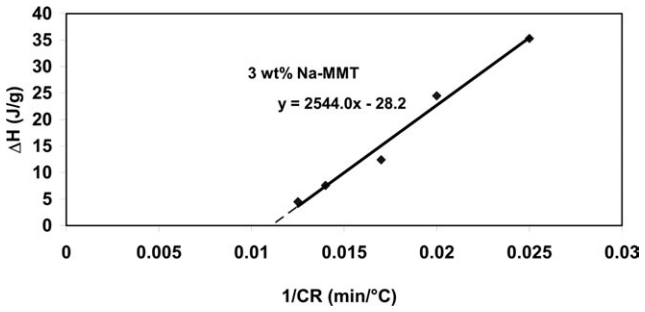

Figure 9. Extrapolated curves of 3wt % MXD6/Na-MMT nanocomposite obtained at cooling rates of 40, 50, 60, 70, and 80°C/min.

Table VIII. Oxygen Permeability of PET and Its Nanocomposites

Sample	Permeability cc*mil/(100*in^2* day*atm)	(% Decrease)
PET	8.7 ± 0.4	-
0.5 wt % PET/Na-MMT	6.2 ± 0.3	(28.7%)
1 wt % PET/Na-MMT	5.1 ± 0.3	(41.4%)
2 wt % PET/Na-MMT	4.2 ± 0.3	(51.7%)
3 wt % PET/Na-MMT	5.2 ± 0.4	(40.2%)
5 wt % PET/Na-MMT	5.5 ± 0.5	(36.8%)

Comparisons of the oxygen permeability (PO_2) values of amorphous films of MXD6 and its nanocomposites are given in Table IX. The PO_2 value of the MXD6 was 0.512 cc*mil/(100*in^2*day*atm). All the MXD6/Na-MMT nanocomposites had lower PO_2 value than the neat MXD6, indicating improvement in their oxygen barrier properties. With 2 wt % clay loading in the MXD6 matrix, PO_2 was decreased to 0.225 cc*mil/(100*in^2*day*atm). The greatest improvement was achieved with the 3 wt % MXD6/Na-MMT nanocomposite, giving a 70% reduction in the PO_2 value. All the results are consistent with TEM observations, with samples exhibiting higher degrees of exfoliation providing better barrier properties. Ammala and Lawrence[84] reported the effects of different organo-modifiers (Cloisite 30B, 10A, and 93A) on oxygen barrier properties of MXD6. They found that the Cloisite 10A additive provided the best oxygen barrier, indicating a PO_2 reduction of 66% compared with the neat MXD6.

CONCLUSIONS

In this work, we have shown that exfoliation of Na-MMT can be achieved in both PET and MXD6 nanocomposites, through the novel melt blending process that was developed. The importance of this blending process is that the polymer nanocomposite consists of Na-MMT and polymer without any surfactants and additives. Because of the high compatibility between water and Na-MMT, the silicate layers of the clay can be dispersed at a nanometer level into the polymer matrices, after removal of the water. At higher clay loading, however, it was difficult to obtain completely exfoliated PET nanocomposites by this method.

Table IX. Oxygen Permeability of MXD6 and Its Nanocomposites

Samples	Permeability cc*mil/(100*in^2* day*atm)	(% decrease)
MXD6	0.512 ± 0.002	-
2 wt % MXD6/Na-MMT	0.225 ± 0.002	(56.3%)
3 wt % MXD6/Na-MMT	0.153 ± 0.004	(70.3%)
5 wt % MXD6/Na-MMT	0.160 ± 0.003	(68.7%)

PET nanocomposites containing nominal concentrations of 0.5, 1, and 2 wt % Na-MMT were well exfoliated, as could be seen in TEM photomicrographs. Upon increasing the Na-MMT content of the PET/Na-MMT nanocomposites up to 3 and 5 wt %, intercalated silicate layers appeared to form mixed morphologies of intercalation and exfoliation. In the case of MXD6 nanocomposites, well exfoliated morphologies were achieved with 2, 3, and 5 wt % clay addition. The TEM evidence shows that a predominately exfoliated structure has been achieved. In this study, in addition to exfoliation, the disappearance of the characteristic XRD peak may also be related to high levels of intercalation, exfoliation, or mixed morphology. These results indicate that XRD should be combined with TEM technologies to characterize the dispersion structures of clay platelets into polymers.

The introduction of Na-MMT appeared to hinder the mobility of polymer chains as it caused slight increases in the glass transition and T_m of the PET nanocomposites. During the reheating and cooling processes, Na-MMT acted as a nucleating agent, which accelerated rates of crystallization. Among the PET/Na-MMT and MXD6/Na-MMT nanocomposites with different weight percent of Na-MMT, the formation of well exfoliated morphology resulted in similar crystallization behaviors. With improved clay dispersion in the polymer matrix, oxygen barrier properties were improved by 50% for PET/Na-MMT and 70% for MXD6/Na-MMT nanocomposites.

REFERENCES

1. Yano, K.; Usuki, A.; Okada, A.; Kuruachi, T.; Kamigato, O. J. *Polym. Sci. Part A: Polym. Chem.* **1997**, *35*, 2289.
2. Bharadwaj, R. K.; Mehrabi, A. R.; Hamilton, C.; Trujillo, C. *Polymer* **2002**, *43*, 3699.
3. Dennis, H. R.; Hunter, D. L.; Chang, D.; Kim, S. *Polymer* **2001**, *42*, 9513.
4. Cheng, L.; Zheng, L.; Li, G.; Zeng, J.; Yin, Q.; Li, R. *Physica B: Condens. Matter* **2008**, *403*, 2584.
5. Velasco, J. I.; Ardanuy, M.; Realinho, V. J. *Appl. Polym. Sci.* **2006**, *102*, 1213.
6. Barrioz, J. C.; Ferry, L.; Frihi, D.; Cavalier, K.; Vigier, G. J. *Appl. Polym. Sci.* **2006**, *100*, 989.
7. Christopher, J. G.; Plummer, M. M.; Béguelin, P.; Orange, G.; Varlet, J. *Polymer* **2004**, *45*, 1147.
8. Tomer, V.; Polizos, G.; Randall, C. A.; Manias, E. J. *Appl. Phys.* **2011**, *109*, 074113.
9. Mittal, V. *Materials* **2009**, *2*, 992.
10. Utracki, L. A.; Kamal, M. R. *Arabian J. Sci. Eng.* **2002**, *27*, 43.
11. Azeredo, H. M. C. *Food Int.* **2009**, *42*, 1240.
12. Ray, S.; Quek, S.; Easteal, A.; Chen, X. D. *Int. J. Food Eng.* **2006**, *2*, 1149.
13. Adame, D.; Beall, G. W. *Appl. Clay Sci.* **2009**, *42*, 545.
14. Alexandre, B.; Langevin, D.; Médéric, P.; Aubry, T.; Couderc, H. J. *Membr. Sci.* **2009**, *328*, 186.
15. Rhim, J. W. *Crit. Rev. Food Sci. Nutr.* **2007**, *47*, 411.
16. Chang, J. H.; Mun, M. K. *Polym. Int.* **2007**, *56*, 57.
17. Lee, S. S.; Ma, Y. T.; Rhee, H. W.; Kim, J. K. *Polymer* **2005**, *46*, 2201.
18. Tsai, T. Y.; Li, C. H.; Chang, C. H.; Cheng, W. H. *Adv. Mater.* **2005**, *17*, 1769.
19. Chen, Z. J.; Luo, P. Fu, Q. *Polym. Adv. Technol.* **2009**, *20*, 916.
20. Zhang, L. L.; Xiong, Y. Z.; Qu, E.; Xu, W. J. *J. Appl. Polym. Sci.* **2011**, *122*, 1316.
21. Ghasemi, H.; Carreau, P. J.; Kamal, M. R. *Polym. Eng. Sci.* **2011**, *51*, 1178.
22. Solís, A. S.; Ibarra, I. R.; Estrada, M. R.; Manero, O. *Polym. Eng. Sci.* **2004**, *44*, 1094.
23. Calcagno, C. I. W.; Mariani, C. M.; Teixeria, S. R.; Mauler, R. S. *Polymer* **2007**, *48*, 966.
24. Xu, X. F.; Ding, Y. F.; Qian, Z. Z.; Wang, F. *Polym. Degrad. Stab.* **2009**, *94*, 113.
25. Ou, C. F.; Ho, M. T.; Lin, J. R. *J. Polym. Res.* **2003**, *10*, 127.
26. Ou, C. F.; Ho, M. T.; Lin, J. R. *J. Appl. Polym. Sci.* **2004**, *91*, 140.
27. Kawasumi, M. J. *Polym. Sci. Part A: Polym. Chem.* **2004**, *42*, 819.
28. Luo, J. J.; Daniel, I. M. *Compos. Sci. Technol.* **2003**, *63*, 1607.
29. Tsai, J. L.; Sun, C. T. *J. Compos. Mater.* **2004**, *38*, 567.
30. Kim, S. G.; Lofgren, E. A.; Jabarin, S. A. *J. Appl. Polym. Sci.* **2013**, *127*, 2201.
31. Calderon, J. U.; Lennox, B.; Kamal, M. *Appl. Clay Sci.* **2008**, *40*, 90.
32. Hotta, S.; Paul, D. R. *Polymer* **2004**, *45*, 7639.
33. Fornes, T. D.; Yoon, P. J.; Paul, D. R. *Polymer* **2003**, *44*, 7545.
34. Dennis, H. R.; Hunter, D. L.; Chang, D.; Kim, S.; White, J. L.; Cho, J. W. *Polymer* **2001**, *42*, 9513.
35. Davis, C. H.; Mathias, L. J.; Gilman, J. W.; Schiraldi, D. A. *J. Polym. Sci. Part B: Polym. Phys.* **2002**, *40*, 2661.
36. Giraldi, A. L. F.; Bizarria, M. T. M.; Silva, A. A.; Mei, L. H. I. *J. Appl. Polym. Sci.* **2008**, *108*, 2252.
37. Chang, J. H.; Mun, M. K.; Lee, I. C. *J. Appl. Polym. Sci.* **2005**, *98*, 2009.
38. Wang, Y. M.; Gao, J. P.; Ma, Y. Q. *Composites B* **2006**, *37*, 399.
39. Scaffaro, R.; Botta, L.; Ceraulo, M.; Mantia, F. P. *J. Appl. Polym. Sci.* **2011**, *122*, 384.
40. Chang, J. H. *Polym. Plast. Technol. Eng.* **2008**, *47*, 791.
41. Jabarin, S. A. In Polymeric Materials Encyclopedia; Salome, J.C., Ed.; CRC: Boca Raton, FL, **1996**; Vol.*8*, pp 6078 and 6091.
42. Jabarin, S. A. *Polym. Eng. Sci.* **1984**, *24*, 376.
43. Carlston, E. F.; Lum, F. G. *J. Ind. Eng. Chem.* **1957**, *49*, 1239.
44. Doudou, B. B.; Dargent, E.; Grenet, J. J. *Plast. Film Sheet* **2005**, *21*, 233.
45. Tung, J.; Gupta, R. K.; Simon, G. P.; Edward, G. H.; Bhattacharya, S. N. *Polymer* **2005**, *46*, 10405.

46. Pospiech, D.; Korwitz, A.; Komber, H.; Voigt, D.; Jehnichen, D. *High Perform. Polym.* **2007**, *19*, 565.
47. Magniez, K.; Fox, B. L.; Looney, M. G. *J. Polym. Sci. Part B: Polym. Phys.* **2009**, *47*, 1300.
48. Chen, Z. J.; Luo, P.; Fu, Q. *Polym. Adv. Technol.* **2009**, *20*, 916.
49. Ammala, A.; Hill, A. J. *J. Appl. Polym. Sci.* **2007**, *104*, 1377.
50. Chung, J. W.; Son, S. B.; Chun, S. W.; Kang, T. J.; Kwak, S. Y. *Polym. Degrad. Stab.* **2008**, *93*, 252.
51. Osman, M. A.; Ploetze, M. J. *Mater. Chem.* **2003**, *13*, 2359.
52. Hwang, S. Y.; Lee, W. D.; Lim, J. S. *J. Polym. Sci. Part B: Polym. Phys.* **2008**, *46*, 1022.
53. Yin, M.; Li, C. C.; Guan, G. H. *J. Appl. Polym. Sci.* **2009**, *114*, 2327.
54. Kim, K. H.; Huh, J. *Macro Res.* **2007**, *15*, 178.
55. Labde, R.; Lofgren, E. A.; Jabarin, S. A. *J. Appl. Polym. Sci.* **2012**, *125*, E693.
56. Strawhecker, K. E.; Manias, E. *Chem. Mater.* **2000**, *12*, 2943.
57. Cho, J. W.; Paul, D. R. *Polymer* **2001**, *42*, 1083.
58. Zhao, Q.; Samulski, E. T. *Polymer* **2006**, *47*, 663.
59. Choi, W. J.; Kim, H. J.; Yoon, K. H.; Hwang, C. J. *Appl. Polym. Sci.* **2006**, *100*, 4875.
60. Ammala, A.; Bell, C.; Dean, K. *Compos. Sci. Technol.* **2008**, *68*, 1328.
61. Eckel, D. F.; Balogh, M. P.; Fasulo, P. D.; Rodgers, W. R. *J. Appl. Polym. Sci.* **2004**, *93*, 1110.
62. Morgan, A. B.; Gilman, J. W. *J. Appl. Polym. Sci.* **2003**, *87*, 1329.
63. Patro, T. U.; Khakhar, D.V.; Misra, A. J. *Appl. Polym. Sci.* **2009**, *113*, 1720.
64. Wahit, M. U.; Hassan, A. J. *Thermoplastics Compos. Mater.* **2006**, *19*, 545.
65. Run, M. T.; Wu, Z.; Zhang, D. Y. *Polymer* **2005**, *46*, 5308.
66. Mitsubishi Gas Chemical Company. Available at: http://www.mgc-a.com/Pages/MXD6/hist-mxd6.html, **2004**.
67. Mucha, M.; Marsza, J.; Fidrych, A. *Polymer* **2000**, *41*, 4137.
68. Fornes, T. D.; Paul, D. R. *Polymer* **2003**, *44*, 3945.
69. Lincoln, D. M.; Vaia, R. A.; Krishnamoorti, R. *Macromolecules* **2004**, *37*, 4554.
70. Magniez, K.; Fox, B. L.; Looney, M. G. *J. Polym. Sci. Part B: Polym. Phys.* **2009**, *47*, 1300.
69. Mucha, M.; Marsza, J.; Fidrych, A. *Polymer* **2000**, *41*, 4137.
71. Calcagno, C, I. W.; Mariani, C. M.; Mauler, R. S. *J. Appl. Polym. Sci.* **2009**, *111*, 29.
72. Hahm, W. G.; Myung, H. S. *Macromol. Res.* **2004**, *12*, 85.
73. Ren, M. Q.; Song, J. B.; Zhao, Q. X.; Li, Y. S. *Polym. Int.* **2004**, *53*, 1658.
74. Ghasemi, H.; Carreau, P. J.; Kamal, M. R. *Polym. Eng. Sci.* **2012**, *52*, 372.
75. Tian, X. Y.; Ruan, C. J.; Cui, P.; Zheng, J. J. *Macromol. Sci. Phys.* **2006**, *45*, 835.
76. Tjong, S. C.; Bao, S. P. *J. Polym. Sci.* **2004**, *42*, 2878.
77. Liu, Z. J. *Polym. Eng. Sci.* **2004**, *44*, 479.
78. Wu, T. M.; Hsu, S. F.; Chien, C. F.; Wu, J. Y. *Polym. Eng. Sci.* **2004**, *44*, 2288.
79. Nowacki, R.; Monasse, B.; Piorkowska, E.; Haudin, J. M. *Polymer* **2004**, *45*, 4877.
80. Gorrasi, G.; Tammaro, L.; Mariarosaria, T.; Vittoria, V.; Kaempfer, D. J. *Polym. Sci. Part B: Polym. Phys.* **2003**, *41*, 1798.
81. Karian, H. G. Handbook of Polypropylene and Polypropylene composites; Marcel Dekker: New York, **2003**.
82. Ray, S. S.; Okamoto, M. *Prog. Polym. Sci.* **2003**, *28*, 1539.
83. Ghasemi, H.; Carreau, P. J.; Kamal, M. R. *Polym. Eng. Sci.* **2012**, *52*, 420.
84. Ammala, A.; Lawrence, K. A. *J. Mater. Chem.* **2008**, *18*, 911.
85. Gatos, K. G. *Eur. Polym. J.* **2007**, *43*, 1097.
86. Kim, S. H.; Kim, S. C. *J. Appl. Polym. Sci.* **2007**, *103*, 1262.
87. Frounchi, M.; Dourbash, A. *Macromol. Mater. Eng.* **2009**, *294*, 68.